Received March 16, 2021, accepted April 30, 2021, date of publication May 10, 2021, date of current version May 20, 2021.

Digital Object Identifier 10.1109/ACCESS.2021.3078884

Reconfigurable Intelligent Surface-Aided Single-Input Single-Output K-Complex Symbol Golden Codeword-Based Modulation

NARUSHAN PILLAY, (Member, IEEE), AND HONGJUN XU, (Member, IEEE)
School of Engineering, University of KwaZulu-Natal, Durban 4041, South Africa
Corresponding author: Narushan Pillay (pillayn@ukzn.ac.za)

ABSTRACT Small reconfigurable intelligent surfaces (RISs) have greater potential for flexibility and ubiquity compared to large RISs. In the literature, the theoretical average bit error probability (ABEP) of a phase-adjustable element access-point-based RIS (AP-RIS) is derived by exploiting the central-limit theorem for large surface size. Hence, the analysis does not hold for small surface sizes. In this paper, we first formulate a simple closed-form expression for the ABEP of a phase-adjustable element AP-RIS with M-ary quadrature amplitude modulation (MQAM). Compared to the results available in literature, this expression is valid even for small RISs. Second, we investigate AP-RIS-aided single-input single-output K-complex symbol Golden codeword-based modulation, which encodes/transmits K MQAM symbols in each of K consecutive independently faded time slots. The encoding ensures that each symbol experiences K different fadings, hence resulting in a K-fold increase in diversity order, while the AP-RIS maximizes the received signal-to-noise ratio (SNR) in each slot and yields significant SNR gains with increasing size. An increase in K yields significant SNR gains for small RISs. A theoretical bound on the ABEP is formulated and validated by simulation. Finally, a detector based on sorted symbol set sphere decoding is devised.

INDEX TERMS Access-point-based reconfigurable intelligent surfaces, intelligent reflecting surfaces, intelligent phase-adjustable surfaces, single-input single-output Golden codeword-based modulation, small intelligent surfaces, sorted symbol set sphere decoding.

I. INTRODUCTION

Reconfigurable intelligent surfaces (RISs) [1] modify the propagation environment to enhance communication system objectives, such as reliability, capacity, security, energy and spectrum efficiency [2]. A traditional RIS is composed of a large number of low-cost and energy-efficient reflecting elements which are associated with an adjustable parameter, for instance, amplitude, phase, frequency or polarisation [2].

A comprehensive survey of RISs was presented in [3], where contributions were categorized into capacity analyses, power/spectral efficiency optimisation, channel estimation, security, energy transfer, terminal implementation and positioning. Phase-adjustable element RISs [2]–[4] have gained the most attention due to their passive and low-cost potential and may be used to improve error performance by maximizing the received signal-to-noise ratio (SNR).

The associate editor coordinating the review of this manuscript and approving it for publication was Anandakumar Haldorai.

Several of the practical challenges of RISs were highlighted in [4]. For example, the acquisition of channel state information (CSI) was identified as a key challenge due to the cascaded channel scenario. Furthermore, in [5], it was pointed out that hardware impairments (HWI) represent a stumbling block to the realization of RIS-aided systems and can be quite severe in typical RIS systems due to the large surface area involved.

Meanwhile, due to the attractive distance properties of the Golden code, which is a full-rate full-diversity space-time block code, Xu et *al.* [6] proposed a generalized form of the Golden code, known as the multiple complex symbol Golden code (MCSGC). Based on the use of $n \geq 1$, $n \in \mathbb{Z}$ embedding encodings at the transmitter, the MCSGC employs two transmit antennas to transmit $K = 2^n$ complex input symbols in each of K consecutive time slots. Assuming a Rayleigh frequency-flat fading channel which changes from one time slot to the next, since every input symbol experiences K different fadings, a diversity order of KN_R is realized for a receiver equipped with N_R antennas.

Motivation: Due to their large size, traditional RISs naturally pose several difficulties which will affect deployment and flexibility. The acquisition of CSI was identified as a considerable challenge [4]. On this note, by assuming the close coupling of an RIS with a radio-frequency source, Basar [7] formulated an access point (AP)-based RIS, which allows for both information transmission and intelligent phase adjustment. Unlike the conventional or non-AP-based RIS, the AP-RIS only requires CSI corresponding to the single receive antenna-RIS element link, and yields a significant SNR gain over its counterpart. HWI which limits the real-world potential of RISs was another challenge identified as possibly severe for large RISs [5]. This motivates that small AP-RISs will render deployment relatively easy, while being more accessible/ubiquitous, due to their ease of placement on small objects like vehicles, furniture and clothing. Further, small RISs will contribute to low-complexity system design and fewer HWIs. However, small RISs trade-off gains in error performance.

In [8], it was demonstrated that the distance properties of the Golden code could be exploited by the transmission of a pair of Golden codeword super-symbols, while using only a single transmit antenna over two consecutive time slots. Then by the application of component-interleaving between pairs of super-symbols, additional diversity gain was realized by the transmission of the interleaved super-symbols over four consecutive time slots. This motivates that the key idea of the MCSGC [6] may be extended to a single transmit antenna system; hence, based on $n \geq 1$, $n \in \mathbb{Z}$ encodings, $K = 2^n$ complex input symbols may be transmitted using only a single transmit antenna in each of K consecutive time slots, which will allow significant improvement in error performance.

Furthermore, with the aim of improving the error performance of small AP-RIS-aided communications which employ single antennas at the transmitter and receiver, we are motivated to investigate RIS-aided single-input single-output (SISO) K-complex symbol Golden codeword based-modulation (RIS-SISO-KCSGCM).

Contributions: The contributions of this paper are as follows: a) An accurate simple closed-form expression of the average bit error probability (ABEP) for an AP-RIS with M-ary quadrature amplitude modulation (MQAM) that is valid even for small RISs is formulated. b) We apply the concept of MCSGC encoding to a single-input system and further propose an AP-RIS-aided SISO-KCSGCM scheme that enhances the error performance of the conventional AP-RIS especially for small RISs. c) A theoretical bound on the ABEP of the scheme is formulated. d) Finally, sorted symbol set sphere decoding detection is devised for the proposed scheme.

Notation: Upper-case bold symbols represent sets or matrices, while lower-case bold symbols represent vectors. The operators $|\cdot|$, $\|\cdot\|_F$, $(\cdot)^T$ and $(\cdot)^H$ represents the Euclidean norm, Frobenius norm, transpose and Hermitian, respectively. $E\{\cdot\}$ is the expectation operator, while $\mathcal{D}(\cdot)$, $Q(\cdot)$ represents the constellation demodulation function and Gaussian Q-function, respectively. argsort $(\boldsymbol{\delta})$ returns the set of indices corresponding to the elements of $\boldsymbol{\delta}$ sorted in ascending order. $(\cdot)!$ represents factorial and $(2N-1)!! = (2N-1)(2N-3)\cdots 3\cdot 1$ represents the double factorial. $j = \sqrt{-1}$ is a complex number.

II. THEORETICAL ABEP FOR AP-RISs WITH MQAM

Assume the transmission of a symbol u, drawn from the set Ω of MQAM symbols with $E\{|u|^2\} = 1$, by an N-element AP-RIS to a single receive antenna, then the received signal assuming a Rayleigh frequency-flat fading channel and the presence of additive white Gaussian noise (AWGN) at the receiver, is given as:

$$y = \left[\sum_{i=1}^{N} h_i e^{j\phi_i}\right] u + \eta, \tag{1.1}$$

$$= \sum_{i=1}^{N} \alpha_i u + \eta, \tag{1.2}$$

where the $C\mathcal{N}(0,\ 1)$ distributed random variable (RV) $h_i = \alpha_i e^{j\theta_i}$ with magnitude α_i and phase θ_i represents the channel between the receive antenna and the i-th RIS element, $\phi_i = -\theta_i$ is the intelligently adjusted [7] phase set at the i-th RIS element and η is the $C\mathcal{N}(0,\ \frac{1}{\bar{\gamma}})$ distributed RV representing AWGN, where $\bar{\gamma}$ is the average SNR at the receive antenna.

The central-limit theorem (CLT), which allows the probability density function (PDF) of $z = \sum_{i=1}^{N} \alpha_i$ for large N to follow a Gaussian distribution is assumed in the literature [7], causing the ABEP analysis to fail for small values of N. However, in [9], [10], the PDF of the sum of Rayleigh distributed RVs was given, hence an expression for the ABEP that is more accurate for small values of N may be formulated as follows.

Let $\varphi = \frac{3N\bar{\gamma}}{M-1}$, $a = \frac{\sqrt{M}-1}{\sqrt{M}}$ and $\alpha = \frac{4a}{\log_2 M}$, then the ABEP for the AP-RIS with MQAM may be formulated as [11]:

$$P_e = \alpha \int_0^{\infty} \left\{ Q\left(\sqrt{\varphi x^2}\right) - aQ^2\left(\sqrt{\varphi x^2}\right)\right\} f_Z(x)\mathrm{d}x, \tag{2}$$

where $f_Z(x)$ the PDF of $Z = z/\sqrt{N}$ may be given[1] as [9], [10]:

$$f_Z(x) = \frac{x^{2N-1} e^{\frac{-x^2}{2b}}}{2^{N-1} b^N (N-1)!}, \tag{3}$$

with $b = \frac{1}{2N}[(2N-1)!!]^{\frac{1}{N}}$.

Let $\alpha_1 = \frac{\alpha}{12(2^{N-1})b^N(N-1)!}$, and employing the well-known approximations $Q(\sqrt{v}) \leq \frac{1}{12}e^{\frac{-v}{2}} + \frac{1}{4}e^{\frac{-2v}{3}}$ and $Q^2(\sqrt{v}) \leq \frac{1}{8}e^{-v}$, (2) may be written as:

$$P_e \approx \alpha_1 \int_0^{\infty} \left(e^{-\beta_{11}x^2} + 3e^{-\beta_{12}x^2} - \frac{3}{2}ae^{-\beta_{13}x^2}\right) x^{2N-1}\mathrm{d}x, \tag{4}$$

[1] A more accurate expression for the PDF of Z was given in [10] but negligible difference was evident in this study.

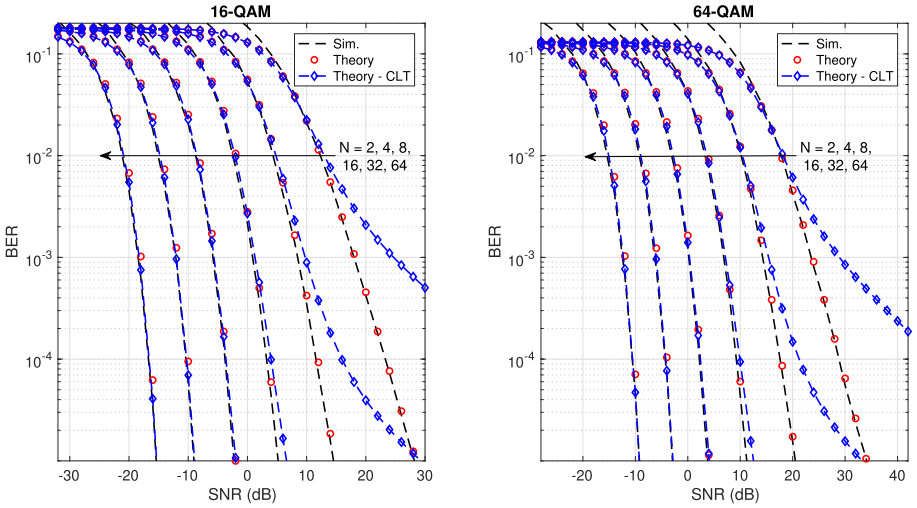

FIGURE 1. Validation of error performance for AP-RISs ($N = 2, 4, 8, 16, 32$ and 64) with $M = 16$ and $M = 64$.

where $\beta_{11} = \frac{b\varphi+1}{2b}$, $\beta_{12} = \frac{2b\varphi+\frac{3}{2}}{3b}$ and $\beta_{13} = \frac{b\varphi+\frac{1}{2}}{b}$.

Using Equ. (3.326.2) in [12], (4) is finally reduced to:

$$P_e \approx \frac{1}{2}\alpha_1\Gamma(N)\Big(\beta_{11}^{-N} + 3\beta_{12}^{-N} - \frac{3}{2}a\beta_{13}^{-N}\Big). \tag{5}$$

Figure 1 demonstrates the simulation results for an AP-RIS with $M = 16$ and 64 for $N = 2, 4, 8, 16, 32$ and 64. The theoretical ABEP curves based on (5) and that of the CLT are also included. The results confirm that the accuracy of (5) is superior when the CLT method fails for $N = 2, 4$ and 8.

A Note on the Diversity Order: At high SNRs, (5) may be approximated as:

$$P_e \approx \frac{1}{2}\alpha_1\Gamma(N)\left[\left(\frac{\varphi}{2}\right)^{-N} + 3\left(\frac{2\varphi}{3}\right)^{-N} - \frac{3}{2}a\varphi^{-N}\right], \tag{6.1}$$

$$= c\bar{\gamma}^{-N}, \tag{6.2}$$

where c is a constant.

It is immediately evident that the diversity order achieved by the AP-RIS is N, the number of elements in the RIS.

III. RIS-AIDED SISO-KCSGCM

A. SYSTEM MODEL

Consider a single antenna N-element AP-RIS transmitter and a single antenna receiver as depicted in Figure 2.

The ℓ-th, $\ell \in [1 : K]$,[2] $\{K = 2^n, n \geq 1, n \in \mathbb{Z}\}$ m-tuple vector $\mathbf{b}_\ell = \left[b_1^\ell\ b_2^\ell \cdots b_p^\ell\right]$ of $p = \log_2 M$ input bits is mapped to the set Ω of MQAM symbols to yield symbol $u_{0,\ell}$, $E\{|u_{0,\ell}|^2\} = 1$. The K symbols are then encoded. The k-th, $k \in [1 : n]$ encoding is given by [6]:

$$u_{k,2m-1} = \frac{\alpha}{\sqrt{5}}\left(u_{k-1,m} + u_{k-1,m+2^{n-1}}\theta\right), \tag{7.1}$$

$$u_{k,2m} = \frac{\bar{\alpha}}{\sqrt{5}}\left(u_{k-1,m} + u_{k-1,m+2^{n-1}}\bar{\theta}\right), \tag{7.2}$$

[2]Note, in this paper we only consider $K = 2$, 4 and 8.

where $m \in [1 : 2^{n-1}]$, $\theta = \frac{1+\sqrt{5}}{2}$, $\bar{\theta} = 1 - \theta$, $\alpha = 1 + j\bar{\theta}$ and $\bar{\alpha} = 1 + j\theta$.

The super-symbols $u_{n,\ell}$ from the n-th encoding are then transmitted over K consecutive time slots by the AP-RIS Transmitter, which has an adjustable phase ϕ_i^ℓ at the i-th, $i \in [1 : N]$ RIS element and ℓ-th time slot. Assuming Rayleigh frequency-flat fading channels $h_i^\ell = \alpha_i^\ell e^{j\theta_i^\ell}$, $\ell \in [1 : K]$ which change from one time-slot to the next, with distribution $C\mathcal{N}(0, 1)$; the phase at the i-th RIS element in the ℓ-th time slot is set as $\phi_i^\ell = -\theta_i^\ell$, such that the received SNR is maximized [7]. Accordingly, the received signal may be defined as:

$$y_\ell = \Big[\sum_{i=1}^{N} h_i^\ell e^{j\phi_i^\ell}\Big]u_{n,\ell} + \eta_\ell = z_\ell u_{n,\ell} + \eta_\ell, \quad \ell \in [1 : K], \tag{8}$$

where $z_\ell = \sum_{i=1}^{N}\alpha_i^\ell$, η_ℓ is the $C\mathcal{N}(0, \frac{1}{\bar{\gamma}})$ distributed RV representing AWGN in the ℓ-th time slot with $\bar{\gamma}$ the average received SNR.

As an example of the encoding (refer Figure 2), consider $K = 4$, then with $n = 2$, $k \in [1 : 2]$ and $m \in [1 : 2]$, using (7.1) and (7.2), after the second encoding we have:

$$\{u_{2,1}, u_{2,2}\} = \left\{\frac{\alpha}{\sqrt{5}}(u_{1,1} + u_{1,3}\theta), \frac{\bar{\alpha}}{\sqrt{5}}(u_{1,1} + u_{1,3}\bar{\theta})\right\}, \tag{9.1}$$

$$\{u_{2,3}, u_{2,4}\} = \left\{\frac{\alpha}{\sqrt{5}}(u_{1,2} + u_{1,4}\theta), \frac{\bar{\alpha}}{\sqrt{5}}(u_{1,2} + u_{1,4}\bar{\theta})\right\}. \tag{9.2}$$

Given the transmission of $u_{2,\ell}$, since the pairs $u_{1,\ell}$, $\ell \in [1, 3]$ and $u_{1,\ell}$, $\ell \in [2, 4]$ each carries all the input symbols $u_{0,\ell}$, $\ell \in [1 : 4]$ (refer Figure 2), every input symbol experiences K fading channels over K time slots.

B. THEORETICAL BOUND ON ABEP

Using vector notation for the received signals, (8) may be expressed in terms of the transmission of MQAM symbols as:

$$\mathbf{y} = \mathbf{H}\mathbf{u} + \mathbf{n}, \tag{10}$$

where $\mathbf{y} = [y_1\ y_2 \cdots y_K]^T$ is of dimension $K \times 1$, $\mathbf{H}$ is a $K \times K$ channel matrix, which may be validated as (11), as shown at the bottom of the page, for $K = 2$, 4 and 8, $\mathbf{u} = [u_{0,1}\ u_{0,2} \cdots u_{0,K}]^T$ is a $K \times 1$ vector of MQAM symbols and $\mathbf{n} = [\eta_1\ \eta_2 \cdots \eta_K]^T$ is of dimension $K \times 1$. Equ. (10) is used in the ensuing analysis and sphere decoding in the next subsection. To simplify the error analysis, we assume that only a single transmitted MQAM symbol $u_{0,1}$ is detected in error, while the remaining symbols are detected correctly [6]. The ℓ-th received signal in (10), may then be defined as:

$$y_\ell = \beta_\ell z_\ell u_{0,1} + \eta_\ell, \quad \ell \in [1:K], \tag{12}$$

where β_ℓ for $K = 2$, 4 and 8 is given as:

$$\begin{bmatrix} \beta_1 & \beta_2 & \cdots & \beta_K \end{bmatrix} = \begin{cases} \frac{1}{\sqrt{5}}[\alpha\ \bar{\alpha}], & \text{if } K = 2, \\ \frac{1}{5}[\alpha^2\ \alpha\bar{\alpha}\ \alpha\bar{\alpha}\ \bar{\alpha}^2], & \text{if } K = 4, \\ \frac{1}{5\sqrt{5}}[\alpha^3\ \alpha^2\bar{\alpha}\ \alpha^2\bar{\alpha}\ \alpha\bar{\alpha}^2\ \alpha^2\bar{\alpha}\ \alpha\bar{\alpha}^2\ \alpha\bar{\alpha}^2\ \bar{\alpha}^3], & \\ \qquad\qquad \text{if } K = 8. \end{cases} \tag{13}$$

Now (12) is equivalent to the transmission of $u_{0,1}$ over K identical fading channels, each with transmit power $|\beta_\ell|^2$. Hence, the ABEP may be given as [11]:

$$P_e \approx \alpha \int_0^{\pi/2} \prod_{\ell=1}^{K} M_{\gamma_\ell}(g_\phi)\mathrm{d}\phi - \alpha a \int_0^{\pi/4} \prod_{\ell=1}^{K} M_{\gamma_\ell}(g_\phi)\mathrm{d}\phi, \tag{14}$$

where $\alpha = \frac{4a}{\pi \log_2 M}$, $a = \frac{\sqrt{M}-1}{\sqrt{M}}$, $M_{\gamma_\ell}(\cdot)$ is the moment generating function (MGF) of the instantaneous SNR γ_ℓ for the ℓ-th fading channel and $g_\phi = -\frac{3}{2(M-1)\sin^2\phi}$.

By employing transformation of RVs and using (3), the PDF of γ_ℓ may be determined. Let $\gamma_\ell = g(Z_\ell)$, where $\gamma_\ell = Z_\ell^2 N|\beta_\ell|^2\bar{\gamma}$ from (12) and $Z_\ell = z_\ell/\sqrt{N}$, then using $g^{-1}(\gamma_\ell) = \sqrt{\frac{\gamma_\ell}{N|\beta_\ell|^2\bar{\gamma}}}$ and $\frac{\mathrm{d}Z_\ell}{\mathrm{d}\gamma_\ell} = \frac{1}{2Z_\ell N|\beta_\ell|^2\bar{\gamma}}$, the PDF $f_{\gamma_\ell}(\gamma_\ell)$ is given as:

$$f_{\gamma_\ell}(\gamma_\ell) = f_{Z_\ell}(g^{-1}(\gamma_\ell))\left|\frac{\mathrm{d}Z_\ell}{\mathrm{d}\gamma_\ell}\right| = \frac{\gamma_\ell^{N-1} e^{-\frac{\gamma_\ell}{2bN|\beta_\ell|^2\bar{\gamma}}}}{(2bN|\beta_\ell|^2\bar{\gamma})^N (N-1)!}. \tag{15}$$

Next, determining the MGF of γ_ℓ [11]:

$$\begin{aligned} M_{\gamma_\ell}(s) &= \frac{1}{(2bN|\beta_\ell|^2\bar{\gamma})^N (N-1)!} \int_0^\infty \gamma_\ell^{N-1} \\ &\quad \times e^{-\left(\frac{1}{2bN|\beta_\ell|^2\bar{\gamma}} - s\right)\gamma_\ell} \mathrm{d}\gamma_\ell \\ &= \frac{\Gamma(N)}{(N-1)!(1-2bN|\beta_\ell|^2\bar{\gamma}s)^N}. \end{aligned} \tag{16}$$

The ABEP defined as (14) is then given as:

$$\begin{aligned} P_e \approx \frac{\alpha\Gamma(N)}{(N-1)!}\Big[&\prod_{\ell=1}^{K} \int_0^{\pi/2} (1 - 2bN|\beta_\ell|^2\bar{\gamma}g_\phi)^{-N}\mathrm{d}\phi \\ &- a\prod_{\ell=1}^{K} \int_0^{\pi/4} (1 - 2bN|\beta_\ell|^2\bar{\gamma}g_\phi)^{-N}\mathrm{d}\phi\Big]. \end{aligned} \tag{17.1}$$

Finally, using the trapezoidal rule to solve, (17.1) may be written as:

$$\begin{aligned} P_e \approx \frac{\alpha\Gamma(N)}{2n(N-1)!}\Big\{ &\prod_{\ell=1}^{K} \Big[\frac{\pi}{2} f(\pi/2) + \pi \sum_{k=1}^{n-1} f\Big(\frac{k\pi}{2n}\Big)\Big] \\ &- a\prod_{\ell=1}^{K} \Big[\frac{\pi}{4} f(\pi/4) + \frac{\pi}{2} \sum_{k=1}^{n-1} f\Big(\frac{k\pi}{4n}\Big)\Big]\Big\}, \end{aligned} \tag{17.2}$$

$$\mathbf{H} = \begin{cases} \frac{1}{\sqrt{5}} \begin{bmatrix} z_1\alpha & z_1\alpha\theta \\ z_2\bar{\alpha} & z_2\bar{\alpha}\bar{\theta} \end{bmatrix}, & \text{if } K = 2, \\ \frac{1}{5} \begin{bmatrix} z_1\alpha^2 & z_1\alpha^2\theta & z_1\alpha^2\theta & z_1\alpha^2\theta^2 \\ z_2\alpha\bar{\alpha} & z_2\alpha\bar{\alpha}\bar{\theta} & z_2\alpha\bar{\alpha}\theta & z_2\alpha\bar{\alpha}\theta\bar{\theta} \\ z_3\alpha\bar{\alpha} & z_3\alpha\bar{\alpha}\theta & z_3\alpha\bar{\alpha}\bar{\theta} & z_3\alpha\bar{\alpha}\theta\bar{\theta} \\ z_4\bar{\alpha}^2 & z_4\bar{\alpha}^2\bar{\theta} & z_4\bar{\alpha}^2\bar{\theta} & z_4\bar{\alpha}^2\bar{\theta}^2 \end{bmatrix}, & \text{if } K = 4, \\ \frac{1}{5\sqrt{5}} \begin{bmatrix} z_1\alpha^3 & z_1\alpha^3\theta & z_1\alpha^3\theta & z_1\alpha^3\theta^2 & z_1\alpha^3\theta & z_1\alpha^3\theta^2 & z_1\alpha^3\theta^2 & z_1\alpha^3\theta^3 \\ z_2\alpha^2\bar{\alpha} & z_2\alpha^2\bar{\alpha}\bar{\theta} & z_2\alpha^2\bar{\alpha}\theta & z_2\alpha^2\bar{\alpha}\theta\bar{\theta} & z_2\alpha^2\bar{\alpha}\theta & z_2\alpha^2\bar{\alpha}\theta\bar{\theta} & z_2\alpha^2\bar{\alpha}\theta^2 & z_2\alpha^2\bar{\alpha}\theta^2\bar{\theta} \\ z_3\alpha^2\bar{\alpha} & z_3\alpha^2\bar{\alpha}\theta & z_3\alpha^2\bar{\alpha}\bar{\theta} & z_3\alpha^2\bar{\alpha}\theta\bar{\theta} & z_3\alpha^2\bar{\alpha}\theta & z_3\alpha^2\bar{\alpha}\theta^2 & z_3\alpha^2\bar{\alpha}\theta\bar{\theta} & z_3\alpha^2\bar{\alpha}\theta^2\bar{\theta} \\ z_4\alpha\bar{\alpha}^2 & z_4\alpha\bar{\alpha}^2\bar{\theta} & z_4\alpha\bar{\alpha}^2\bar{\theta} & z_4\alpha\bar{\alpha}^2\bar{\theta}^2 & z_4\alpha\bar{\alpha}^2\theta & z_4\alpha\bar{\alpha}^2\theta\bar{\theta} & z_4\alpha\bar{\alpha}^2\theta\bar{\theta} & z_4\alpha\bar{\alpha}^2\theta\bar{\theta}^2 \\ z_5\alpha^2\bar{\alpha} & z_5\alpha^2\bar{\alpha}\theta & z_5\alpha^2\bar{\alpha}\theta & z_5\alpha^2\bar{\alpha}\theta^2 & z_5\alpha^2\bar{\alpha}\bar{\theta} & z_5\alpha^2\bar{\alpha}\theta\bar{\theta} & z_5\alpha^2\bar{\alpha}\theta\bar{\theta} & z_5\alpha^2\bar{\alpha}\theta^2\bar{\theta} \\ z_6\alpha\bar{\alpha}^2 & z_6\alpha\bar{\alpha}^2\bar{\theta} & z_6\alpha\bar{\alpha}^2\theta & z_6\alpha\bar{\alpha}^2\theta\bar{\theta} & z_6\alpha\bar{\alpha}^2\bar{\theta} & z_6\alpha\bar{\alpha}^2\bar{\theta}^2 & z_6\alpha\bar{\alpha}^2\theta\bar{\theta} & z_6\alpha\bar{\alpha}^2\theta\bar{\theta}^2 \\ z_7\alpha\bar{\alpha}^2 & z_7\alpha\bar{\alpha}^2\theta & z_7\alpha\bar{\alpha}^2\bar{\theta} & z_7\alpha\bar{\alpha}^2\theta\bar{\theta} & z_7\alpha\bar{\alpha}^2\bar{\theta} & z_7\alpha\bar{\alpha}^2\theta\bar{\theta} & z_7\alpha\bar{\alpha}^2\bar{\theta}^2 & z_7\alpha\bar{\alpha}^2\theta\bar{\theta}^2 \\ z_8\bar{\alpha}^3 & z_8\bar{\alpha}^3\bar{\theta} & z_8\bar{\alpha}^3\bar{\theta} & z_8\bar{\alpha}^3\bar{\theta}^2 & z_8\bar{\alpha}^3\bar{\theta} & z_8\bar{\alpha}^3\bar{\theta}^2 & z_8\bar{\alpha}^3\bar{\theta}^2 & z_8\bar{\alpha}^3\bar{\theta}^3 \end{bmatrix}, & \text{if } K = 8 \end{cases} \tag{11}$$

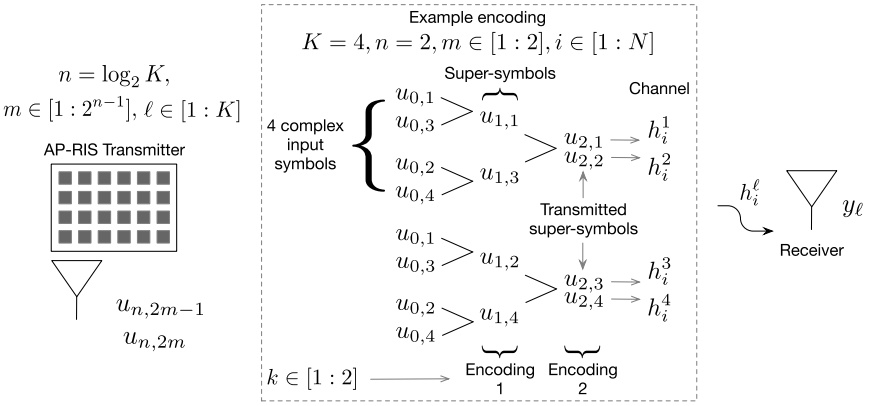

FIGURE 2. System model of the proposed RIS-aided SISO-K CSGCM including example encoding for $K = 4$.

where $f(\phi) = (1 - 2bN|\beta_\ell|^2\bar{\gamma}g_\phi)^{-N}$ and $n = 10$ is the number of partitions employed in the numerical integration. Note, setting $K = 1$ and $\beta_1 = 1$ in (17.2) will yield an alternate result for the theoretical ABEP of an AP-RIS with MQAM compared to (5).

A Note on the Diversity Order: At high SNRs, (17.1) may be approximated as:

$$P_e \approx \frac{\alpha\Gamma(N)}{(N-1)!}\prod_{\ell=1}^{K}\int_0^{\pi/2}(-2bN|\beta_\ell|^2\bar{\gamma}g_\phi)^{-N}\mathrm{d}\phi. \quad (18.1)$$

Upper-bounding (18.1) by setting $\phi = \frac{\pi}{2}$, we have:

$$P_e \approx \frac{\alpha\pi\Gamma(N)}{2(N-1)!}\left(\frac{3bN\bar{\gamma}}{M-1}\right)^{-KN}\prod_{\ell=1}^{K}|\beta_\ell|^{-2N}. \quad (18.2)$$

It is immediately evident that the diversity order of the RIS-SISO-KCSGCM scheme is KN and is significantly larger than the diversity order of the AP-RIS [7] scheme, which may be determined as N by setting $K = 1$.

C. SORTED SYMBOL SET SPHERE DECODING

Based on (10), employing the QR decomposition of $\mathbf{H}$, $\mathbf{H} = \mathbf{QR}$, and multiplying both sides of (10) by $\mathbf{Q}^H$ we have:

$$\mathbf{z} = \mathbf{Q}^H\mathbf{y} = \mathbf{Ru} + \tilde{\mathbf{n}} = [z(1) \quad z(2) \quad \cdots \quad z(K)]^T, \quad (19)$$

where $\mathbf{Q}$ is a $K \times K$ unitary matrix, $\mathbf{R}$ is a $K \times K$ upper-triangular matrix with (i,j)-th entry $r(i,j)$, $\tilde{\mathbf{n}} = \mathbf{Q}^H\mathbf{n}$ and $\mathbf{z}$ is a $K \times 1$ vector. Based on the radius of sphere decoding r [13], the decoding is then based on: $\|\mathbf{z} - \mathbf{Ru}\|_F^2 \leq \mathrm{r}^2$, hence the steps adapted from [6] are given as:

Step 1: Calculate $\mathbf{z}$ based on (19).

Step 2: Determine the estimated MQAM symbols $\tilde{u}_{0,\ell}$, $\ell \in [1:K]$ in reverse order:

$$\tilde{u}_{0,K} = \mathcal{D}\Big(v_K = \frac{z(K)}{r(K,K)}\Big), \quad (20.1)$$

$$\tilde{u}_{0,\ell} = \mathcal{D}\Big(v_\ell = \frac{z(\ell) - \sum_{i=\ell+1}^{K} r(\ell,i)\tilde{u}_{0,i}}{r(\ell,\ell)}\Big), \quad \ell \in [1:K-1]. \quad (20.2)$$

Step 3: Sort all symbols in the MQAM constellation set Ω from the most to least probable transmission to yield the sorted symbols $u_{0,\ell}^q$, $q \in [1:M]$:

$$[u_{0,\ell}^1 \quad u_{0,\ell}^2 \quad \cdots \quad u_{0,\ell}^M] = \Omega(\mathrm{argsort}\,(\delta_1^\ell, \delta_2^\ell, \cdots, \delta_M^\ell)), \quad (21)$$

where $\delta_q^\ell = |v_\ell - u_0^q|^2$, $\ell \in [1:K]$, $q \in [1:M]$ and $u_0^q \in \Omega$.

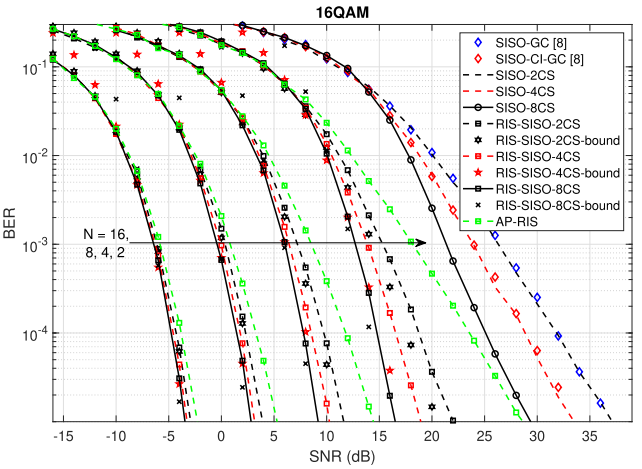

FIGURE 3. Error performance comparison of the proposed schemes for $M = 16$ and $N = 2, 4, 8$ and 16.

Step 4: Detect the K transmitted symbols using sorted symbol set sphere decoding.

The K-th symbol $\hat{u}_{0,K}$ is determined by using the constraint:

$$|z(K) - r(K,K)u_{0,K}^{\tilde{q}}|^2 \leq \mathrm{r}^2, \quad (22.1)$$

where $\tilde{q} \in [1:L]$ and L, $1 < L \leq M$ is the most probable transmitted symbols for a given SNR.[3]

Let $p_K(\hat{u}_{0,K}) = z(K) - r(K,K)\hat{u}_{0,K}$ and $p_\ell(x) = z(\ell) - r(\ell,\ell)x - \sum_{i=\ell+1}^{K} r(\ell,i)\hat{u}_{0,i}$, $\ell \in [1:K-1]$, then each of the remaining ℓ, $\ell \in [1:K-1]$ MQAM symbols are determined

[3]Note, smaller values of L are chosen for the lower SNRs [6]. The values of L used in the simulations are specified in Section IV.

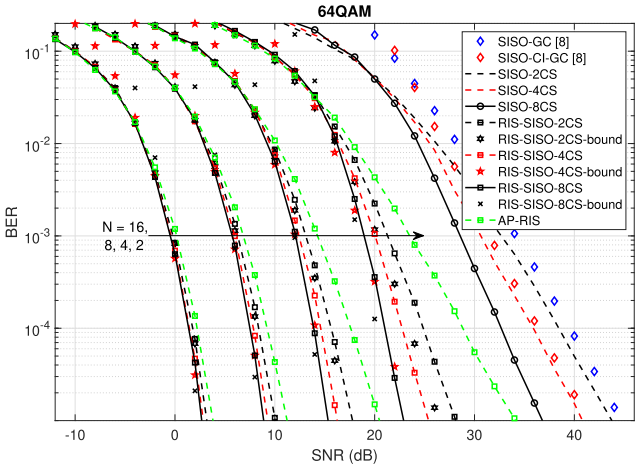

FIGURE 4. Error performance comparison of the proposed schemes for $M = 64$ and $N = 2$, 4, 8 and 16.

in reverse order using the constraint:

$$|p_\ell(u_{0,\ell}^{\tilde{q}})|^2 \leq \mathrm{r}^2 - \sum_{i=\ell+1}^{K} |p_i(\hat{u}_{0,i})|^2. \tag{22.2}$$

IV. NUMERICAL RESULTS

In this section, the numerical results for the SISO-KCSGCM and RIS-aided SISO-KCSGCM schemes for $K = 2$, 4 and 8 are presented. We denote the non-RIS schemes as SISO-2CS, -4CS and -8CS and the RIS-aided schemes as RIS-SISO-2CS, -4CS and -8CS. For error performance comparisons, the figure-of-merit considered is the bit error rate (BER) versus average SNR. Comparisons are drawn at a BER of 10^{-5}. We consider $N = 2$, 4, 8 and 16. The values of L are shown in Tables 1 and 2 (refer to top of Page 7). The bound on the ABEP given by (17.2) is included. We also draw comparison with the two schemes presented in [8] for the SISO setting and the AP-RIS scheme of [7].

TABLE 1. Simulation settings of L for SISO-KCS.

M	K	SISO-KCS
16	2	SNR= [0:2:16, 18, 20:2:24, 26, 28:2:32, 34:2:38] L=[2, 4, 8, 10, 15, 16]
	4	SNR= [0:2:6, 8:2:12, 14:2:16, 18, 20, 22:2:24, 26:2:28, 30:2:34] L=[2, 4, 6, 8, 10, 12, 14, 16]
	8	SNR= [0:2, 4:2:12, 14:2:16, 18, 20, 22:2:24, 26:2:30] L=[2, 4, 6, 8, 12, 14, 16]
64	2	SNR=[0:2:12, 14:2:20, 22, 24, 26:2:30, 32:2:34, 36, 38, 40:2:42, 44:2:46] L=[2, 4, 6, 8, 10, 20, 30, 34, 60, 64]
	4	SNR=[0:2:16, 18:2:26, 28:2:32, 34, 36, 38, 40:2:46] L=[2, 10, 30, 40, 58, 60, 64]
	8	SNR=[0:2:14, 16:2:18, 20:2:22, 24, 26, 28, 30:2:32, 34:2:40] L=[2, 8, 10, 16, 20, 26, 40, 64]

In Figure 3, the results for $M = 16$ are presented, while Figure 4 presents the corresponding results for $M = 64$. For $M = 64$, the results for the schemes of [8] are evaluated using the theoretical ABEP (cf. Equs. (15) and (16) in [8]) due to very long simulation time.

For both $M = 16$ and $M = 64$, as expected it is evident that the SISO-2CS and -4CS schemes agree well with the schemes of [8], while the SISO-8CS schemes yields a significant SNR gain. For example, compared to SISO-CI-GC [8], gains of approximately 4 dB and 5 dB are realized for $M = 16$ and 64, respectively. The RIS-aided schemes yield significant improvement in error performance over their counterparts. Consider $M = 16$. For $N = 2$, compared to SISO-2CS, -4CS and -8CS, the corresponding RIS-aided schemes yield SNR gains of 14.8 dB, 14.4 dB and 12.7 dB, respectively. For $N = 4$, the SNR gains are 25 dB, 22.7 dB and 20 dB, respectively. With $N = 8$ and $N = 16$, the corresponding gains are 32.4 dB, 29.7 dB, 26.2 dB and 39.3 dB, 36.2 dB, 32.4 dB, respectively.

Similar gains are evident for $M = 64$. In comparison to AP-RIS, for $M = 16$ and $N = 2$, RIS-SISO-2CS yields an SNR gain of 6.8 dB, while the -4CS and -8CS configurations yield gains of 9.8 dB and 12.3 dB. For $N = 4$, the corresponding SNR gains are 3 dB, 4.2 dB and 5.2 dB, respectively. Employing $N = 8$ and $N = 16$, SNR gains of 1.3 dB, 2 dB, 2.5 dB and 0.77 dB, 1.1 dB, 1.24 dB, respectively, are yielded. Similar gains are evident for $M = 64$. Hence, the largest gains are evident for small values of N. In all instances, it is shown

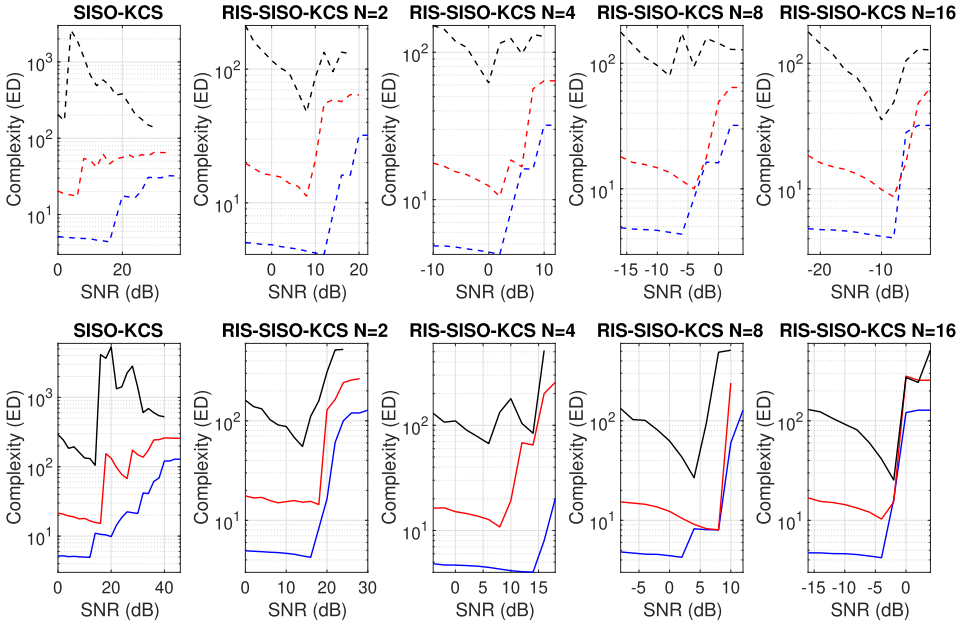

FIGURE 5. Complexity comparison of proposed SISO-KCS and RIS-SISO-KCS schemes for $K = 2$ (blue), $K = 4$ (red) and $K = 8$ (black) with $M = 16$ (dashed) and $M = 64$ (solid).

TABLE 2. Simulation settings of L for RIS-SISO-KCS.

M	K	RIS-SISO-KCS			
		$N=2$	$N=4$	$N=8$	$N=16$
16	2	SNR=[-6:2:12, 14, 16:2:18, 20:2:22] L=[2, 4, 8, 16]	SNR=[-10:2:2, 4, 6:2:8, 10:2:12] L=[2, 4, 8, 16]	SNR=[-16:2:-6, -4, -2:2:0, 2:2:4] L=[2, 4, 8, 16]	SNR=[-22:2:-8, -6, -4:2:-2] L=[2, 14, 16]
	4	SNR=[-6:2:8, 10, 12, 14:2:16, 18:2:20] L=[2, 4, 12, 14, 16]	SNR=[-10:2:2, 4:2:6, 8, 10:2:12] L=[2, 4, 14, 16]	SNR=[-16:2:-4, -2, 0, 2:2:4] L=[2, 4, 12, 16]	SNR=[-22:2:-8, -6, -4, -2] L=[2, 4, 12, 16]
	8	SNR=[-6:2:8, 10, 12:2:14, 16:2:18] L=[2, 4, 10, 16]	SNR=[-10:2:0, 2, 4, 6, 8:2:10] L=[2, 4, 8, 10, 16]	SNR=[-16:2:-8, -6:2:-4, -2, 0:2:4] L=[2, 4, 12, 16]	SNR=[-22:2:-10, -8, -6, -4:2:-2] L=[2, 4, 12, 16]
64	2	SNR=[0:2:16, 18, 20, 22, 24, 26:2:28, 30] L = [2, 4, 8, 30, 50, 60, 64]	SNR=[-4:2:14, 16, 18, 20, 22:2:24, 26] L = [2, 4, 10, 30, 60, 64]	SNR=[-8:2:2, 4:2:8, 10, 12] L = [2, 4, 30, 64]	SNR=[-16:2:-4, -2, 0, 2:2:4] L = [2, 8, 60, 64]
	4	SNR=[0:2:8, 10:2:14, 16, 18:2:20, 22, 24, 26] L = [2, 16, 20, 30, 40, 60, 64]	SNR=[-4:2:8, 10, 12:2:14, 16, 18] L = [2, 4, 16, 50, 64]	SNR=[-8:2:8, 10] L = [2, 60]	SNR=[-16:2:-4, -2, 0:2:4] L = [2, 50, 64]
	8	SNR=[0:2:14, 16, 18, 20, 22, 24] L=[2, 4, 10, 30, 60, 64]	SNR=[-4:2:6, 8, 10:2:14, 16] L=[2, 4, 10, 64]	SNR=[-8:2:4, 6, 8, 10] L=[2, 10, 60, 64]	SNR=[-16:2:-2, 0:2:2, 4] L=[2, 30, 64]

TABLE 3. SNR gains for RIS-SISO-4CS and -8CS compared to RIS-SISO-2CS.

KCS(N)	SNR gain compared to $K=2$ ($M=16$)				SNR gain compared to $K=2$ ($M=64$)			
	2	4	8	16	2	4	8	16
4CS	3.2 dB	1.4 dB	0.8 dB	0.4 dB	2.7 dB	1.5 dB	0.7 dB	0.5 dB
8CS	5.5 dB	2.5 dB	1.2 dB	0.7 dB	5.1 dB	2.5 dB	1.1 dB	0.5 dB

that the bounds agree well with the simulation results and its tightness increases with increasing N.

Finally, we draw comparison between the RIS-SISO-2CS, -4CS and -8CS schemes. The SNR gains are tabulated in Table 3 for $M = 16$ and 64 and it is evident that as N becomes larger, the gains yielded reduce. Hence, varying K is most effective for small values of N.

To summarize, the above investigation demonstrates that the proposed RIS-SISO-KCSGCM scheme represents an attractive option for improving the error performance of small RISs, additionally noting that the effect of increasing K is more effective the smaller the RIS.

Figure 5 shows the computational complexity imposed during detection from simulation for the SISO-KCS and RIS-SISO-KCS schemes. Only the primary contribution to the complexity, i.e. the Euclidean distance (ED) computations in Step 4 is considered [6]. It is evident that the complexities imposed by the SISO-KCS and RIS-SISO-KCS schemes do not differ substantially. In general, as expected, the complexity is highest for $K = 8$ and lowest for $K = 2$. At the low SNRs, the difference between complexities for $K = 2$, 4 and 8 is largest and can be up to an order of magnitude larger, while the difference reduces with increasing SNR. Furthermore, for the RIS schemes, as expected, varying N has minimal effect on complexity.

V. CONCLUSION AND FUTURE WORK

In this paper, the theoretical ABEP of an AP-RIS with MQAM for arbitrary surface sizes was formulated and validated. The evaluated expression agrees well with simulation results even for small RISs. The proposed RIS-SISO-KCSGCM showed a superior BER compared to its non-RIS counterparts. Compared to AP-RIS, and for different values of K, the scheme was most effective for small RISs. A theoretical ABEP bound for the scheme was formulated and validated. Sphere decoding based on a sorted symbol set was proposed. Possible future work is the application of index modulation to the proposed RIS-aided scheme.

REFERENCES

[1] N. Kaina, M. Dupré, G. Lerosey, and M. Fink, "Shaping complex microwave fields in reverberating media with binary tunable metasurfaces," *Sci. Rep.*, vol. 4, no. 1, pp. 1–7, Oct. 2014.

[2] Y.-C. Liang, R. Long, Q. Zhang, J. Chen, H. V. Cheng, and H. Guo, "Large intelligent surface/antennas (LISA): Making reflective radios smart," 2019, *arXiv:1906.06578*. [Online]. Available: http://arxiv.org/abs/1906.06578

[3] J. Zhao and Y. Liu, "A survey of intelligent reflecting surfaces (IRSs): Towards 6G wireless communication networks," 2019, *arXiv:1907.04789*. [Online]. Available: http://arxiv.org/abs/1907.04789

[4] X. Yuan, Y.-J. A. Zhang, Y. Shi, W. Yan, and H. Liu, "Reconfigurable-intelligent-surface empowered wireless communications: Challenges and opportunities," 2020, *arXiv:2001.00364*. [Online]. Available: http://arxiv.org/abs/2001.00364

[5] S. Hu, F. Rusek, and O. Edfors, "Capacity degradation with modeling hardware impairment in large intelligent surface," in *Proc. IEEE Global Commun. Conf. (GLOBECOM)*, Dec. 2018, pp. 1–6.

[6] H. Xu and N. Pillay, "Multiple complex symbol Golden code," *IEEE Access*, vol. 8, pp. 103576–103584, 2020.

[7] E. Basar, "Transmission through large intelligent surfaces: A new frontier in wireless communications," 2019, *arXiv:1902.08463*. [Online]. Available: http://arxiv.org/abs/1902.08463

[8] H. Xu and N. Pillay, "Golden codeword-based modulation schemes for single-input multiple-output systems," *Int. J. Commun. Syst.*, vol. 32, no. 10, p. e3963, Jul. 2019.

[9] M. Schwartz, W. R. Bennett, and S. Stein, *Communication Systems and Techniques*. New York, NY, USA: McGraw-Hill, 1966.

[10] J. Hu and N. C. Beaulieu, "Accurate simple closed-form approximations to Rayleigh sum distributions and densities," *IEEE Commun. Lett.*, vol. 9, no. 2, pp. 109–111, Feb. 2005.

[11] K. Simon and M.-S. Alouini, *Digital Communication Over Fading Channels: A Unified Approach to Performance Analysis*. New York, NY, USA: Wiley, 2000.

[12] I. S. Gradshteyn and I. M. Ryzhik, *Table of Integrals, Series, and Products*, 7th ed. Berkeley, CA, USA: Elsevier, 2007.

[13] B. M. Hochwald and S. T. Brink, "Achieving near-capacity on a multiple-antenna channel," *IEEE Trans. Commun.*, vol. 51, no. 3, pp. 389–399, Mar. 2003.

NARUSHAN PILLAY (Member, IEEE) received the M.Sc. degree *(cum laude)* in engineering and the Ph.D. degree in wireless communications from the University of KwaZulu-Natal, Durban, South Africa, in 2008 and 2012, respectively.

He was with the Council of Scientific and Industrial Research (CSIR), Defence, Peace, Safety and Security (DPSS), South Africa. He has been with the University of KwaZulu-Natal, since 2009. He is also supervises several Ph.D. and M.Sc.Eng. students. He is an NRF-Rated Researcher in South Africa. His research interest includes physical wireless communications, including spectrum sensing for cognitive radio and MIMO systems. He has published several articles in well-known journals in his area of research.

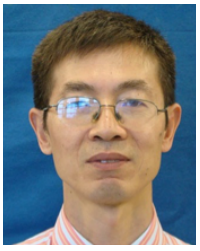

HONGJUN XU (Member, IEEE) received the B.Sc. degree from the Guilin University of Electronic Technology, China, in 1984, and the M.Sc. degree from the Institute of Telecontrol and Telemeasure, China, in 1989, and the Ph.D. degree from the Beijing University of Aeronautics and Astronautics, Beijing, China, in 1995. He was a Postdoctoral Researcher with the University of Natal and Inha University, from 1997 to 2000. He is currently a Full Professor with the School of Engineering, University of KwaZulu-Natal, Howard College Campus. He is also an National Research Foundation (NRF) Rated Researcher, South Africa. He has published more than 50 journal articles. His research interests include digital and wireless communications and digital systems.